JTTEE5 18:187–193
DOI: 10.1007/s11666-009-9302-9
1059-9630/$19.00 © ASM International

Application of Plasma-Sprayed Complex Perovskites as Thermal Barrier Coatings

Maria Ophelia Jarligo, Daniel Emil Mack, Robert Vassen, and Detlev Stöver

(Submitted October 17, 2008; in revised form January 27, 2009)

In an effort to improve the performance of heat engines at high temperatures, advanced surface coatings have been developed from complex perovskites. Materials of $Ba(Mg_{1/3}Ta_{2/3})O_3$ and $La(Al_{1/4}Mg_{1/2}Ta_{1/4})O_3$ composition were synthesized and applied as ceramic topcoats of thermal barrier coating (TBC) systems by atmospheric plasma spraying (APS) in single layer and in double-layer combination with conventional yttria stabilized zirconia (YSZ). Microstructural and phase analyses reveal that plasma spraying of complex perovskites is accompanied with the formation of vertical crack networks and secondary oxide phases which influence the failure mechanism of the TBCs. The low value of fracture toughness for the complex perovskites and the thermally grown oxide at the topcoat-bondcoat interface of the TBCs are, however, the major factors which lead to the coating failure on thermal cycling at about 1250 °C.

Keywords atmospheric plasma spraying, coating properties, complex perovskite, thermal barrier coating (TBC), thermal cycling

1. Introduction

A wide search for new thermal barrier coating (TBC) materials which can improve or substitute the yttria stabilized zirconia (YSZ)-based TBCs has been conducted to increase the operation efficiency of heat engines. Such new TBCs should allow operation temperatures higher than 1200 °C without phase transformation, aside from thermochemical and thermomechanical compatibility with the substrate layer to be coated. Recently, rare-earth perovskites (ABO_3) have been considered for this purpose. Such perovskites are characterized by melting point higher than 1800 °C. Further, the thermal expansion coefficient has values typically greater than 8.5×10^{-6}/K and thermal conductivity of less than 2.2 W/m-K, which are advantageous for use as heat insulating layer (Ref 1, 2).

Among the rare-earth perovskites, the complex $Ba(Mg_{1/3}Ta_{2/3})O_3$ (BMT) and $La(Al_{1/4}Mg_{1/2}Ta_{1/4})O_3$ (LAMT) have recently been investigated. In particular, BMT has been proven as one of the most refractory oxides known to science with melting temperature as high as 3100 °C (Ref 3). Another interesting feature of these material structures is that, the ordering effect in the *B*-site allows for the properties to be tailored (Ref 3-6), making them very attractive candidates for materials development in TBC applications.

At present, several effective processing techniques have been used to deposit different material systems from pyrochlores to perovskites as TBCs (Ref 1, 7-11). Atmospheric plasma spraying (APS) is among those techniques which are capable of effectively depositing high melting temperature materials (Ref 12). With this technique, powders are injected into the plasma where particles are accelerated and melted or partially melted, before they solidify into splats on metallic substrates.

This article reports on the thermal and mechanical properties of the synthesized complex perovskites and their performance as TBC materials, including the driving mechanism that leads to the failure of the TBC on thermal cycling at high temperatures.

2. Experimental Procedure

$Ba(Mg_{1/3}Ta_{2/3})O_3$ and $La(Al_{1/4}Mg_{1/2}Ta_{1/4})O_3$ were synthesized from stoichiometric amounts of $BaCO_3$ (Alfa Aesar, 99.8%), La_2O_3 (Aldrich, 99.9%), Al_2O_3 (Fluka, >95%), MgO (Aldrich, >99%) and Ta_2O_5 (Treibacher Powdermet, 98.95%) powders, mechanically activated in ethanol suspension by planetary ball milling at 150 rpm for 12 h. The milled precursors were dried and calcined at 1250 °C for 3 h prior to final heat treatment at 1600 °C for 4 h. Phases formed were determined by x-ray diffraction analysis.

Bulk specimens $25 \times 5 \times 3$ mm in size were then prepared from the synthesized powders by cold isostatic pressing followed by sintering at 1600 °C for 10 h in air. These specimens were used for dilatometry tests to determine the linear expansion of the complex perovskites up to 1200 °C. Dense cylindrical samples with 10 mm diameter were also prepared by hot pressing at 1600 °C

Maria Ophelia Jarligo, Daniel Emil Mack, Robert Vassen, and **Detlev Stöver**, Institut für Energieforschung (IEF-1), Forschungszentrum Jülich GmbH, 52425 Juelich, Germany. Contact e-mail: m.o.jarligo@fz-juelich.de.

for 3 h with a pressure of ~80 MPa. These samples were used for determination of mechanical properties by depth-sensing microindentation and thermal conductivity from the data of thermal diffusivity by laser flash technique, heat capacity by differential scanning calorimetry and density by Archimedes method. The data gathering procedures are given in detail in Ref 13.

For application as ceramic top coat in TBC systems by APS, powder feeds need to be dense and of good flowability. The synthesized BMT powders exhibited these qualities upon final heat treatment and subsequent mechanical pulverization, but not LAMT. Hence, the LAMT powders were first spray-dried as described in detail in a previous publication (Ref 14). Sieved particles for both perovskite materials with sizes between 45 and 125 μm were utilized for coating by APS using Triplex I gun (Sulzer Metco) operated with flowing Argon and Helium. The complex perovskite powders were coated on disc-shaped nickel-base superalloy IN738 substrates with 150 μm thickness NiCoCrAlY bondcoat deposited by an F4 gun of the vacuum plasma spray facility (Sulzer Metco). Standard steel plates were simultaneously sprayed for characterization of the as-sprayed coatings. The porosity level of the free-standing coatings removed from the steel plates by soaking with HCl, was determined by mercury porosimetry. Phase composition and microstructure of the as-sprayed coatings were analyzed by XRD and SEM, respectively. Double-layer systems consisting of a 7.8 wt.% YSZ coating directly deposited on the bondcoat and a complex perovskite topcoat were also produced. The thickness of each topcoat was about half the total coating thickness of approximately 300 μm.

Gas burner rig facilities were used to determine the thermal cycling lifetime of the TBC systems as described in (Ref 15). In the rigs, the samples were periodically heated and cooled. On heating, the reverse side of the sample was simultaneously cooled by compressed air to maintain a controlled temperature gradient across the samples. After a 5-min high temperature phase, the burner was removed and the sample cooled with compressed air for 2 min. The coating lifetime is the number of thermal cycles at which spallation of about 5×5 mm^2 of the coating could be visible. At least two replicate samples were subjected to burner rig tests to confirm the reliability of results. Metallographic specimens were then cut-out from the cycled samples for microstructural investigation.

3. Results and Discussion

3.1 Bulk Properties

The linear expansion versus temperature profiles as shown in Fig. 1, do not manifest any significant structural change during heating up to 1200 °C for both complex perovskites. The corresponding thermal expansion coefficient (TEC) profiles presented in Fig. 2 show promising values. In particular, TEC values in increasing temperature for BMT are higher than that of 4.4 mol.% YSZ

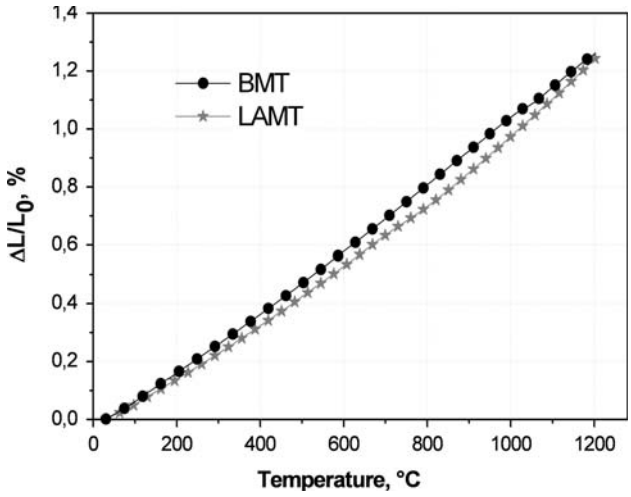

Fig. 1 Linear expansion of BMT and LAMT vs. temperature

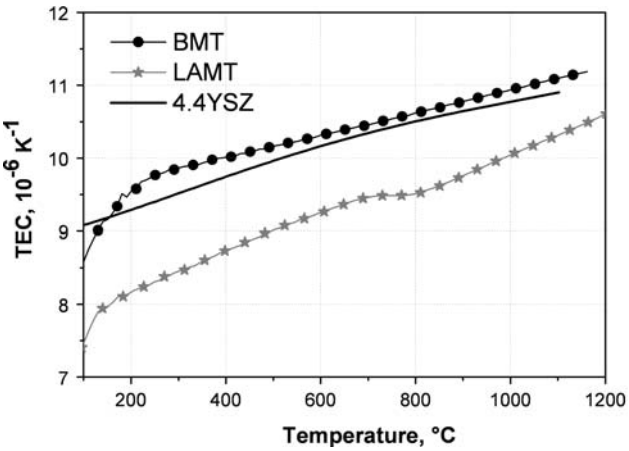

Fig. 2 Thermal expansion coefficient vs. temperature of BMT and LAMT, including 4.4YSZ for comparison

(corresponding to ~7.8 wt.% YSZ) and other new generation TBC materials mentioned in (Ref 10). In fact, they are even higher than the TEC of the single crystal BMT in (Ref 3). With high TEC, the stress misfit between topcoat, bondcoat, and the super alloy substrate can be alleviated during thermal cycling.

Properties of dense samples (~95% relative density) show, that despite higher C_p value at 1200 °C for LAMT (Fig. 3), its much lower thermal diffusivity of 0.0055 cm^2/s as compared to 0.0083 cm^2/s for BMT, resulted to lower thermal conductivity (Fig. 4) at this temperature. The thermal conductivity at 1000 °C for LAMT is even lower than that of 3YSZ and some of the previously published TBC materials (Ref 2, 16, 17). The mechanical properties obtained by micro-indentation tests (Table 1) show elastic modulus lower than that of YSZ (Ref 18), which is quite desirable for TBC applications. In contrast, low values of fracture toughness associated to an inhomogeneity of the material due to the presence of secondary phases, are

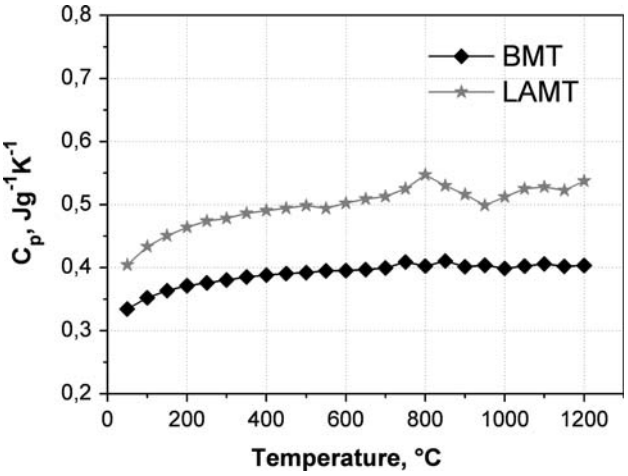

Fig. 3 Heat Capacity vs. temperature of BMT and LAMT

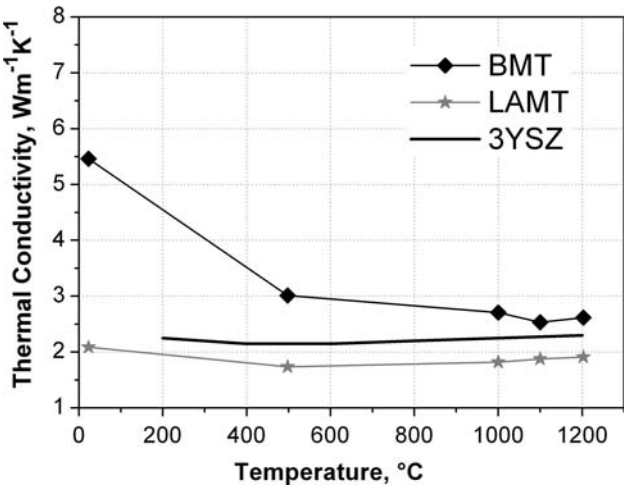

Fig. 4 Thermal conductivity vs. temperature of BMT and LAMT, including 3YSZ for comparison

Table 1 Mechanical properties of the bulk samples

Composition	Young's Modulus, GPa	Hardness, GPa	Fracture toughness, $MPa{\cdot}m^{1/2}$
BMT	186 ± 2	12 ± 2	~0.7
LAMT	174 ± 2	13 ± 2	~0.6
YSZ, *t'phase* (Ref 18)	210 ± 10	13 ± 1	~3

undesirable. Often, the crystallization of complex perovskites at high temperatures is associated with the formation of small amount of secondary phases (Ref 3, 5, 19), which are very stable even after long periods of sintering at extremely high temperatures (Ref 20).

3.2 Plasma-Sprayed Coatings

Several APS parameters were varied to obtain the desirable porosity levels in the coatings. The BMT powder

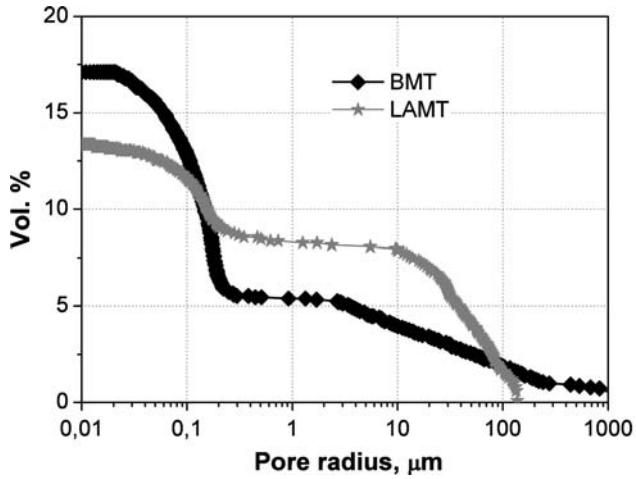

Fig. 5 Mercury porosity measurements of free-standing as-sprayed coatings corresponding to the samples subjected for thermal cycling

was effectively coated on standard steel substrate using a Triplex I gun operated with flowing Ar and He at 20 and 13 standard liter per minute (slpm), respectively. The optimized spray distance of 90 mm produced about 17% total pore volume (Fig. 5) in the ceramic topcoat.

Atmospheric plasma spraying with Triplex I (~300 A operational current) was not able to effectively deposit LAMT on the steel substrates despite varying the spray conditions. The sprayed LAMT powders seemed to have been poorly deposited as they easily fell-off the steel substrate when soaked in HCl solution, and even in plain water. It should be noted that the LAMT powders were previously spray dried, thus the actual particle size is in-fact smaller. In-flight particle, diagnostics is however in progress to determine the state of the LAMT particles during plasma spraying. The failure of depositing LAMT with Triplex I prompted the use of Triplex II gun (~530 A operational current) with a higher operation capability. At a spray distance of 200 mm with flowing Ar and He gas of 45 slpm and 6 slpm, respectively, Triplex II was able to produce LAMT coatings which were successfully removed from the standard steel substrate with hydrochloric acid. The free-standing LAMT coating had about 13% porosity. Obviously, the coatings produced with Triplex II have lower porosity levels owing to the higher power of the plasma gun compared to Triplex I, to melt the powder regardless of the feeding rate. The YSZ coatings used in the double-layer systems had porosity levels of 13-18%.

The micrographs of the plasma-sprayed double-layer coatings are shown in Fig. 6. The microstructures are characterized with microcracks as usually observed in plasma-sprayed coatings. Large intersplat delamination cracks as well as vertical crack networks can be observed in the double-layer YSZ/BMT deposited with Triplex I gun (Fig. 6a). The large cracks running parallel to the coating surface are reducing the bonding between splats, however also decrease the thermal conductivity. Secondary phase forming thin white shades could also be observed in the micrograph of the BMT coating.

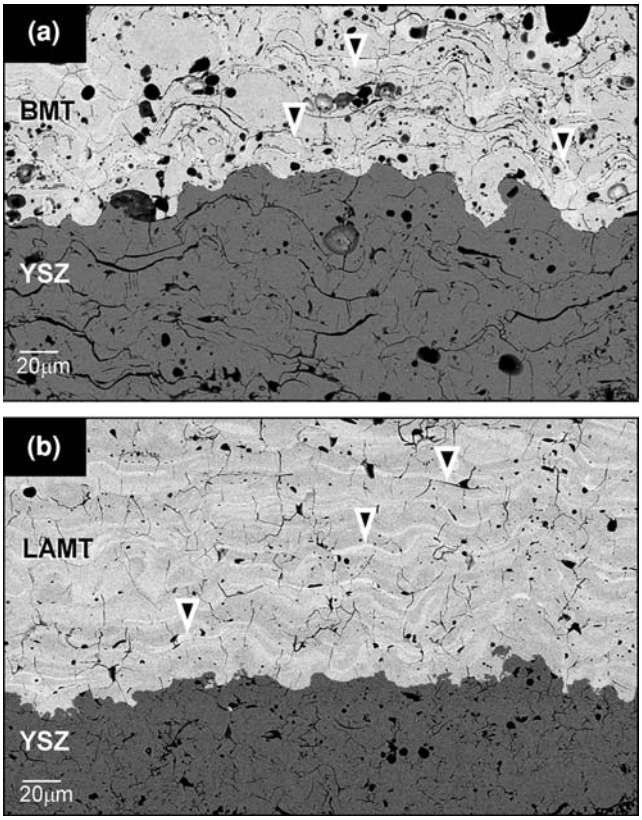

Fig. 6 Cross-section micrographs of (a) BMT/YSZ and (b) LAMT/YSZ double-layer coatings as sprayed using APS

Small broadening in the x-ray diffraction profile at around 30° 2θ in Fig. 7(a) of the as-sprayed BMT, indicates the presence of an amorphous phase. Perovskites were observed to decompose forming secondary phases at high temperatures during particle in-flight on plasma spraying (Ref 11). On EDX analysis, the secondary phase was confirmed to be composed of Ba, Ta, and O.

The occurrence of secondary phase is similarly observed in the micrograph of the as-sprayed LAMT/YSZ topcoat (Fig. 6b), as the XRD profile also reveals a more distinct amorphous peak (Fig. 8a). The LAMT secondary phase forming thin white shades along the splats were determined to be composed of La, Ta, and O by EDX analysis. The microstructure of the as-sprayed LAMT/YSZ double-layer system is characterized by high concentration of finer and denser vertical crack networks and lower porosity level. Intersplat horizontal cracks are hardly visible indicating good intersplat bonding.

On thermal cycling at ~1250 °C surface temperature, no further decomposition of the BMT perovskite was observed, and the associated secondary phase which increased in crystallinity was found to be a $Ba_3Ta_5O_{15}$ (BTO) oxide. However, it was found that the simple disordered cubic structure of the as-sprayed BMT in Fig. 7(a), transformed into an ordered hexagonal structure on thermal cycling (Fig. 7b-c). Corresponding photographs of the cycled TBC coatings made from BMT are shown in Fig. 9.

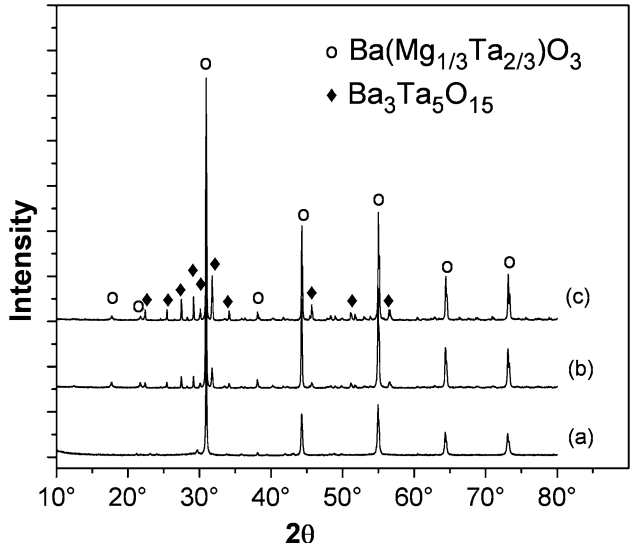

Fig. 7 X-ray diffraction profile of double-layer BMT/YSZ surface (a) as-sprayed, (b) after 560 cycles at 1242 °C/1038 °C, and (c) after 167 cycles at 1339 °C/1003 °C surface/bondcoat temperatures

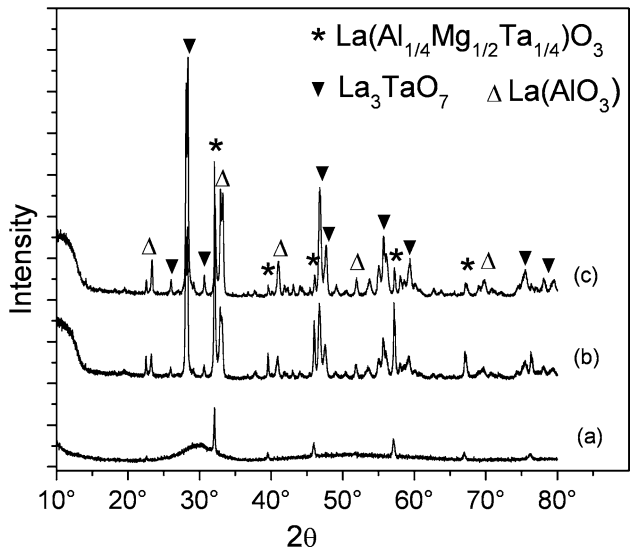

Fig. 8 X-ray diffraction profile of LAMT (a) as-sprayed, (b) in single layer after 527 cycles at 1235 °C/944 °C, and (c) in double-layer with YSZ after 1921 cycles at 1229 °C/999 °C surface/bondcoat temperatures

After 31 cycles at 1215 °C/1022 °C surface/bondcoat temperatures, the single-layer system failed at the topcoat-bondcoat interface, indicating that the failure was oxidation driven although the oxide layer is still rather thin after this short exposure time. This is related to the low toughness of the perovskites (Ref 7). The double-layer system failed within the BMT layer as YSZ was not observed in the XRD profile (Fig. 7c) after 167 cycles at 1339 °C/1003 °C surface/bondcoat temperatures. This indicates that the material capability on exposure at these temperatures is limited. The poor intersplat bonding in the

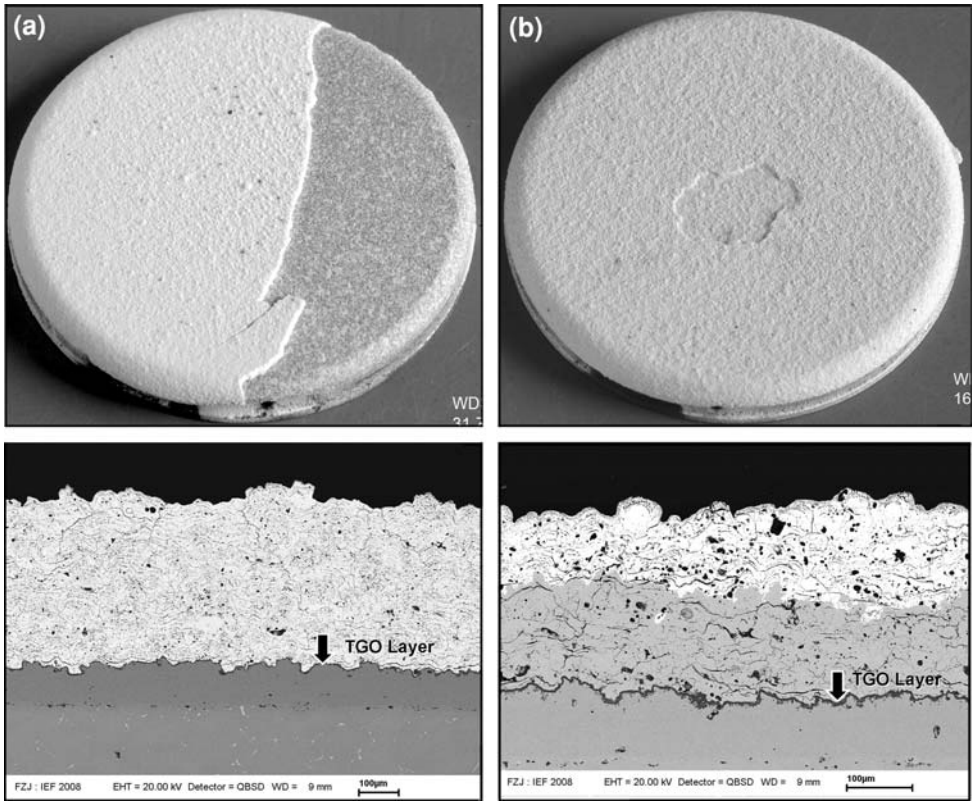

Fig. 9 Photograph and corresponding micrograph (bottom) of BMT in (a) single-layer after 31 cycles at 1215 °C/1022 °C and in (b) double-layer with YSZ after 167 cycles at 1339 °C/1003 °C surface/bondcoat temperatures

BMT layer could have also prevented the relief of the thermal stresses through the large microcracks (Ref 20). In addition, the presence of secondary oxide phase along the splat lines could also contribute to further stress mismatch between the topcoat and the bondcoat on thermal cycling.

On thermal cycling both the single-layer and double-layer systems of LAMT, La_3TaO_7, and $La(AlO_3)$ phases were found to crystallize at ~1250 °C/~1000 °C surface/bondcoat temperatures (Fig. 8b-c). The structure of LAMT remained in cubic form upon thermal cycling, but the orthorhombic La_3TaO_7 and rhombohedral $La(AlO_3)$ phases became more dominant on increasing thermal cycling surface temperature. The lifetime of LAMT coatings particularly the double-layer system, fall within the lifetime range of the standard YSZ TBC in (Ref 7). These coatings have a more promising lifetime compared to BMT coatings despite the low values of fracture toughness. This is probably due to higher concentration of vertical crack networks and good intersplat bonding in the LAMT coatings deposited by Triplex II gun. The vertical crack networks probably performed in similar manner as segmentation cracks, which can greatly improve the strain tolerance of the coatings during thermal cycling. Good intersplat bonding can also effectively avoid delamination failure (Ref 20). However, further oxidation of LAMT during thermal cycling results to formation of secondary oxide phases which may have different values of thermal expansion coefficient than the LAMT main phase. Such occurrence will affect the inter-particle response to thermal stresses during cycling, and ultimately contribute to the total failure of the coating systems as in Fig. 10, which is also oxidation driven from the growth of TGO.

Investigation on the improvement of the properties of these promising TBC systems is currently being pursued as new techniques have surfaced on how to prevent or control the reactions in the perovskite coatings during plasma spraying (Ref 21). Although low values of fracture toughness is responsible for early crack propagation, accordingly, the thermal protection of the component does not deteriorate with the presence of microcracks, conversely the thermal conductivity drops, as long as the cracking mechanism is not catastrophic for the TBC system (Ref 22).

4. Conclusion

Coating systems made of atmospheric plasma-sprayed LAMT complex perovskites show promising TBC performance on high temperature thermal cycling compared to BMT. Plasma spraying of complex perovskites is accompanied with the formation of vertical crack networks and secondary oxide phases which could influence the failure mechanism of the TBCs. Since the means to control the propagation of catastrophic interfacial cracks from thermally grown oxide along the interface of the

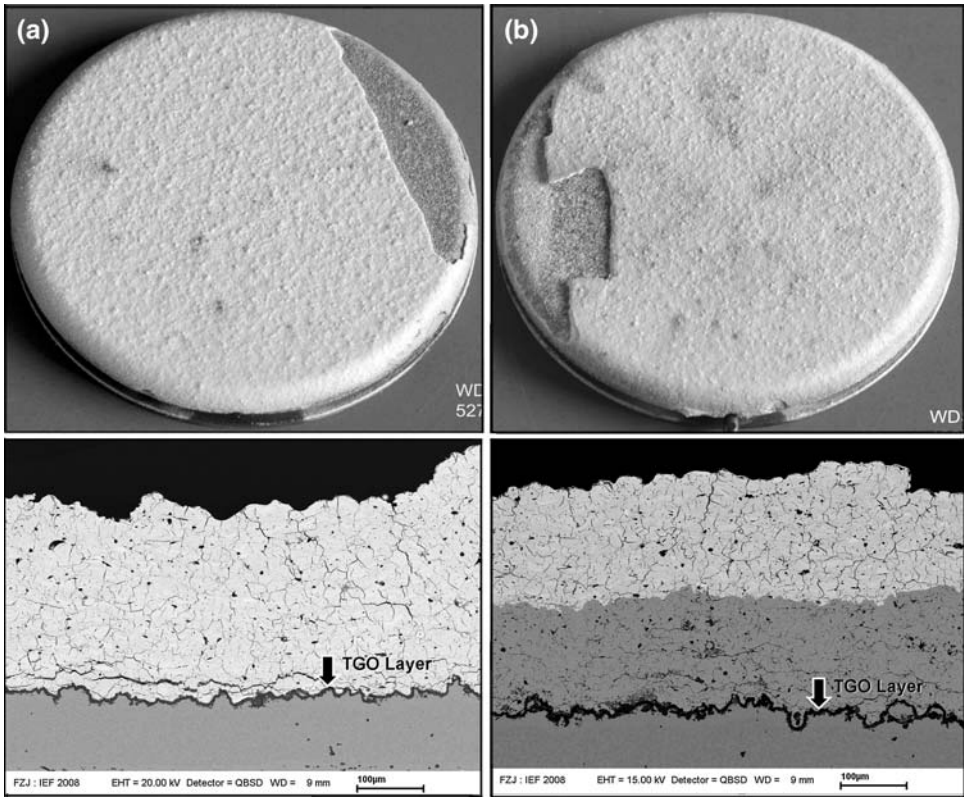

Fig. 10 Photograph and corresponding micrograph (bottom) of LAMT in (a) single-layer after 527 cycles at 1235 °C/944 °C and in (b) double-layer with YSZ after 1921 cycles at 1229 °C/999 °C surface/bondcoat temperatures

coatings are available, the synthesized complex perovskites pose a promising future for new generation TBC materials development.

Acknowledgment

The authors would like to thank Dr. W. Fischer (IEF-2), Dr. J. Malzbender (IEF-2), Mr. D. Pitzer (BN) and to the numerous staff from IEF-1, Forschungszentrum Jülich, Germany, who in one way or another contributed to the fulfillment of this investigation.

References

1. W. Ma, D.E. Mack, R. Vassen, and D. Stöver, Perovskite-type Strontium Zirconate as a New Material for Thermal Barrier Coatings, *J. Am. Ceram. Soc.*, 2008, **91**(8), p 2630-2635
2. T. Maekawa, K. Kurosaki, and S. Yamanaka, Thermal and Mechanical Properties of Perovskite-type Barium Hafnate, *J. Alloys Compd.*, 2006, **407**, p 44-48
3. R. Guo, A.S. Bhalla, and L.E. Cross, $Ba(Mg_{1/3}Ta_{2/3})O_3$ Single Crystal Fiber Grown by the Laser Growth Technique, *J. Appl. Phys.*, 1994, **75**(9), p 4704
4. L. Dupont, L. Chai, and P.K. Davies, A- and B-Site Order in $(Na_{1/2}La_{1/2})$- $(Mg_{1/3}Ta_{2/3})O_3$ Perovskites, *Solid State Chemistry of Inorganic Materials II*, (Pittsburgh, PA), Materials Research Society, 1999
5. C.-C. Tsai and H. Teng, Synthesis of $Ba(Mg_{1/3}Ta_{2/3})O_3$ Microwave Ceramics Through a Sol-gel Route Using Acetate Salts, *J. Am. Ceram. Soc.*, 2004, **87**(11), p 2080-2085
6. T. Shimada, K. Touji, H.-L. Liu, Y.-T. Tzeng, C.-T. Chia, and T. Kolodiazhnyi, Signature of Lattice Defects in Far Infrared Reflectivity of $Ba(Mg_{1/3}Ta_{2/3})O_3$, *J. Eur. Ceram. Soc.*, 2007, **27**, p 2797-2802
7. R. Vaßen, F. Traeger, and D. Stöver, New Thermal Barrier Coatings Based on Pyrochlore/YSZ Double-Layer Systems, *Int. J. Appl. Ceram. Technol.*, 2004, **1**(4), p 351-361
8. X. Ma, F. Wu, J. Roth, M. Gell, and E.H. Jordan, Low Thermal Conductivity Thermal Barrier Coating Deposited by the Solution Plasma Spray Process, *Surf. Coat. Technol.*, 2006, **201**, p 4447-4452
9. J. Wu, X. Wei, N.P. Padture, P.G. Klemens, M. Gell, E. Garcia, P. Miranzo, and M.I. Osendi, Low-Thermal-Conductivity Rare-Earth Zirconates for Potential Thermal-Barrier-Coating Applications, *J. Am. Ceram. Soc.*, 2002, **85**, p 3031-3035
10. H. Lehmann, D. Pitzer, G. Pracht, R. Vassen, and D. Stover, Thermal Conductivity and Thermal Expansion Coefficients of the Lanthanum Rare-Earth-Element Zirconate System, *J. Am. Ceram. Soc.*, 2003, **86**, p 1338-1344
11. C. Monterrubio-Badillo, H. Ageorges, T. Chartier, J.F. Coudert, and P. Fauchais, Preparation of $LaMnO_3$ Perovskite Thin Films by Suspension Plasma Spraying for SOFC Cathodes, *Surf. Coat. Technol.*, 2006, **200**, p 3743-3756
12. P. Fauchais, Understanding Plasma Spraying, *J. Phys. D Appl. Phys.*, 2004, **37**, p R86-R108
13. W. Ma, M.O. Jarligo, D.E. Mack, D. Pitzer, J. Malzbender, R. Vaßen, and D. Stöver, New Generation Perovskite Thermal Barrier Coating Materials, *J. Therm. Spray Technol.*, 2008, **17**(5–6), p 831-837

14. X. Cao, R. Vassen, S. Schwartz, W. Jungen, and D. Stöver, Spray-Drying of Ceramics for Plasma-Spray Coating, *J. Eur. Ceram. Soc.*, 2000, **20**, p 2433-2439
15. F. Traeger, R. Vaßen, K.-H. Rauwald, and D. Stöver, A Thermal Cycling Setup for Thermal Barrier Coatings, *Adv. Eng. Mater.*, 2003, **5**(6), p 429-432
16. N.P. Bansal and D. Zhu, Effects of Doping on Thermal Conductivity of Pyrochlore Oxides for Advanced Thermal Barrier Coatings, *Mater. Sci. Eng. A*, 2007, **459**, p 192-195
17. N.P. Bansal and D. Zhu, Thermal Properties of Oxides with Magnetoplumbite Structure for Advanced Thermal Barrier Coatings, *Surf. Coat. Technol.*, 2008, **202**, p 2698-2703
18. C. Mercer, J.R. Williams, D.R. Clarke, and A.G. Evans, On a Ferroelastic Mechanism Governing the Toughness of Metastable Tetragonal Prime (t') Yttria-Stabilized Zirconia, *Proc. Roy. Soc.*, 2007, **463**, p 1393-1408
19. Y. Fang, A. Hu, S. Ouyang, and J. Jei Oh, The Effect of Calcination on the Microwave Dielectric Properties of $Ba(Mg_{1/3}Ta_{2/3})O_3$, *J. Eur. Ceram. Soc.*, 2001, **21**, p 2745-2750
20. H.B. Guo, R. Vassen, and D. Stoever, Atmospheric Plasma Sprayed Thick Thermal Barrier Coatings with High Segmentation Crack Density, *Surf. Coat. Technol.*, 2004, **186**, p 353-363
21. A. Ansar, G. Schiller, O. Patz, J.B. Gregoire, and Z. Ilhan, Plasma Sprayed Oxygen Electrode for Solid Oxide Fuel Cells and High Temperature Electrolyzers, *Thermal Spray Crossing Borders*, E. Lugscheider, Ed., June 2-4, 2008 (Maastricht, The Netherlands), DVS, 2008, p 871-876
22. A.A. Rubinstein and Y. Tang, Analysis of Crack Nets Development in Thermal Barrier Coatings, *Int. J. Fract.*, 2008, **151**, p 57-79